PHYSICAL REVIEW B **93**, 121402(R) (2016)

Elasticity limits structural superlubricity in large contacts

Tristan A. Sharp,[1,*] Lars Pastewka,[2,1] and Mark O. Robbins[1,†]

[1]*Department of Physics and Astronomy, Johns Hopkins University, 3400 North Charles Street, Baltimore, Maryland 21218, USA*

[2]*Institute for Applied Materials, Karlsruhe Institute of Technology, Engelbert-Arnold-Strasse 4, 76131 Karlsruhe, Germany*

(Received 5 October 2015; revised manuscript received 15 February 2016; published 8 March 2016)

Geometrically imposed force cancellations lead to ultralow friction between rigid incommensurate crystalline asperities. Elastic deformations may avert this cancellation but are difficult to treat analytically in finite and three-dimensional systems. We use atomic-scale simulations to show that elasticity affects the friction only after the contact radius a exceeds a characteristic length set by the core width of interfacial dislocations b_{core}. As a increases past b_{core}, the frictional stress for both incommensurate and commensurate surfaces decreases to a constant value. This plateau corresponds to a Peierls stress that drops exponentially with increasing b_{core} but remains finite.

DOI: 10.1103/PhysRevB.93.121402

Friction is omnipresent but large gaps remain in our understanding of its atomic origins and our ability to control it to reduce energy loss or improve braking. One fascinating phenomenon observed at nanometer scales is structural lubricity, a state of ultralow friction that results from the systematic cancellation of forces across an interface between solids that have no common periodicity [1–3]. Experiments have observed this cancellation between identical crystalline surfaces that are rotated to become incommensurate [2,4–7], different crystalline surfaces [8,9], and between amorphous and crystalline surfaces [9,10]. Superlubricity has been suggested to underlie the mechanism of solid lubrication by plates of graphite and MoS_2 [3,11], and to have the potential to lower friction in a range of applications.

Theoretical treatments of superlubricity have usually considered the limit of rigid solids illustrated in Figs. 1(a) and 1(c). If surfaces share no common period, then atoms sample all relative positions with equal probability in the thermodynamic limit. The resulting energy is translationally invariant and there is no friction. For finite systems the cancellation is incomplete. The frictional stress (force per unit area) scales as a power of the contact radius a for incommensurate and amorphous surfaces, approaching zero as a increases [9,12,13].

The elastic compliance of the surfaces has the potential to dramatically alter superlubricity because atoms move to preferentially sample low energy configurations [Figs. 1(b) and 1(d)]. If elasticity leads to multiple metastable states, there can be finite friction [14–16]. The one-dimensional (1D) case corresponds to the well-studied Frenkel-Kontorova chain model [14]. The infinite chain shows a nonanalytic transition from zero to finite friction with increasing compliance, but finite chains have friction associated with dislocations (solitons) at the chain ends [14]. Several groups have investigated the two-dimensional (2D) case of a compliant monolayer on a rigid substrate [17–20], but there have been comparatively few studies of frictional contacts where compliant three-dimensional objects interact at a two-dimensional interface. It has been suggested that dislocations at the interface could lead to friction [21,22], but Müser found that incommensurate interfaces became unstable to interdiffusion before the friction force becomes finite [23]. Friction due to internal elasticity at incommensurate interfaces has only been observed for a very compliant system with just a few contacting atoms that could lock in multiple metastable states [24].

In this Rapid Communication we study the scaling of friction with compliance and contact size for circular contacts between incommensurate or commensurate crystals. An efficient Green's function method allows us to vary the radius a from less than a nanometer to a fraction of a micrometer. The studies show that there is a transition as a exceeds the core width b_{core} of interfacial dislocations. For $a < b_{\mathrm{core}}$ the frictional stress τ_{fric} is consistent with previous results for rigid surfaces, dropping to zero with increasing a for incommensurate surfaces and remaining constant for commensurate surfaces. For $a > b_{\mathrm{core}}$ compliance leads to new behavior. At intermediate a/b_{core}, τ_{fric} is controlled by dislocation nucleation near the edge of the contact where there is a diverging stress in continuum theory [25]. At large a/b_{core}, τ_{fric} saturates at a finite value that is related to the Peierls stress for dislocation motion. There is never true superlubricity with zero friction. However, the Peierls stress drops exponentially to zero as b_{core} increases and the friction in large contacts may be extremely small.

We consider the simplified geometry of a circular disk interacting with a semi-infinite elastic substrate. This mimics the islands studied by Dietzel *et al.* [9] or contact between a sphere and flat substrate. Separate simulations for the latter geometry exhibit the same behavior reported below. The disk is rigid and the substrate has shear modulus G and Poisson ratio ν. This case can be mapped to contact of two compliant objects in continuum theory [26].

Atoms on both surfaces form a square lattice with nearest-neighbor spacing d, corresponding to (001) surfaces of fcc crystals. The nearest-neighbor direction of the substrate is rotated by an angle θ relative to that of the disk. At $\theta = 0$ the system is commensurate with all atoms in phase. Rotating the system out of alignment by an angle θ creates an incommensurate contact that is similar to a twist grain boundary (Fig. 1). Similar results were obtained with surfaces made incommensurate by changing the lattice constant.

The interaction of the substrate surface atoms with the rigid disk is represented by a simple sinusoidal force in the x-y

*tsharp@pha.jhu.edu
†mr@pha.jhu.edu

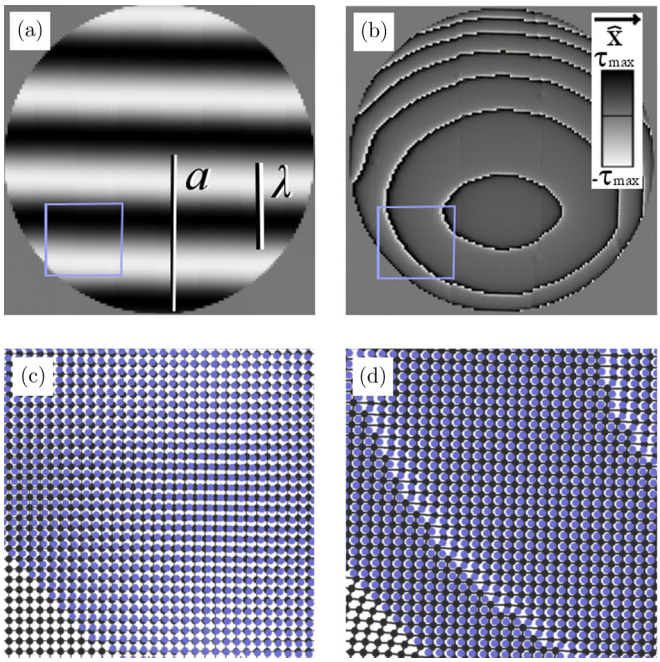

FIG. 1. (a), (b) Grayscale plot of traction in the sliding direction and (c), (d) enlarged view of atomic positions (blue) and energy minima of the substrate potential (gray) for incommensurate crystals with $\theta = 0.03$ rad, $\lambda \sim 33d$, and $a = 62d$. In (a), (c) the substrate is effectively rigid, $G/\tau_{max} = 256$, and all atoms advance together. The traction forces alternate in sign and sum to nearly zero. In (b), (d) the substrate is compliant, $G/\tau_{max} = 1$, and sliding occurs through the motion of dislocations between regions that have locked in registry (see the movie in the Supplemental Material [33]).

plane of the substrate as in the Frenkel-Kontorova chain and two-dimensional Peierls-Nabarro model [14,27],

$$\boldsymbol{f}(x,y) = \tau_{max} d^2[\sin(2\pi x/d)\hat{\boldsymbol{x}} + \sin(2\pi y/d)\hat{\boldsymbol{y}}], \quad (1)$$

for $r < a$, where τ_{max} represents the maximum local frictional stress or traction. The competition between bulk deformation and interfacial slip can be characterized by a core width $b_{core} \equiv dG/\tau_{max}$. For all cases studied, b_{core} equaled the distance from the center of an interfacial edge dislocation to the line where the stress drops to $\tau_{max}/2$.

The displacement of substrate atoms is calculated with a Green's function technique that describes the linear response of a semi-infinite substrate [28–30]. The results presented below are for the commonly studied case of an isotropic substrate with $\nu = 0.5$, but other interactions gave equivalent results [31]. The substrate is displaced quasistatically and the energy minimized after each step using LAMMPS [32]. The static friction is determined from the maximum force between the surfaces during sliding. Normalizing by contact area gives the macroscopic frictional stress τ_{fric}. Results are shown for sliding at $\theta/2$ to the x axis, but other sliding directions give similar scaling.

Figure 1 contrasts the behavior of rigid and compliant substrates for an incommensurate case of $\theta = 0.03$ rad. For the stiff case, substrate atoms remain on an ideal rotated square lattice and atoms are equally likely to be above or between atoms of the disk. The force resisting sliding oscillates as the registry changes with a characteristic period $\lambda \sim d/\theta$ at small angles. The cancellation in forces for $a > \lambda$ leads to structural superlubricity [1–3].

For rigid incommensurate lattices with a circular contact area, the static friction stress has an upper bound that decreases as a power of a, $\tau_{fric} \sim \tau_{max}(a/d)^{-3/2}$ at large a [6,9,13,23]. Figure 2(a) shows the static friction stress of a contact with $\theta = 25°$. When the shear modulus G is large, the friction follows the predicted rigid scaling shown by the dashed line. Elasticity is unimportant since $b_{core} = dG/\tau_{max}$ is much greater than a. Note that there are special radii where the cancellation of forces is nearly exact and the friction is anomalously small compared to the power law fit. To minimize fluctuations, these special radii are not included in Fig. 2(b).

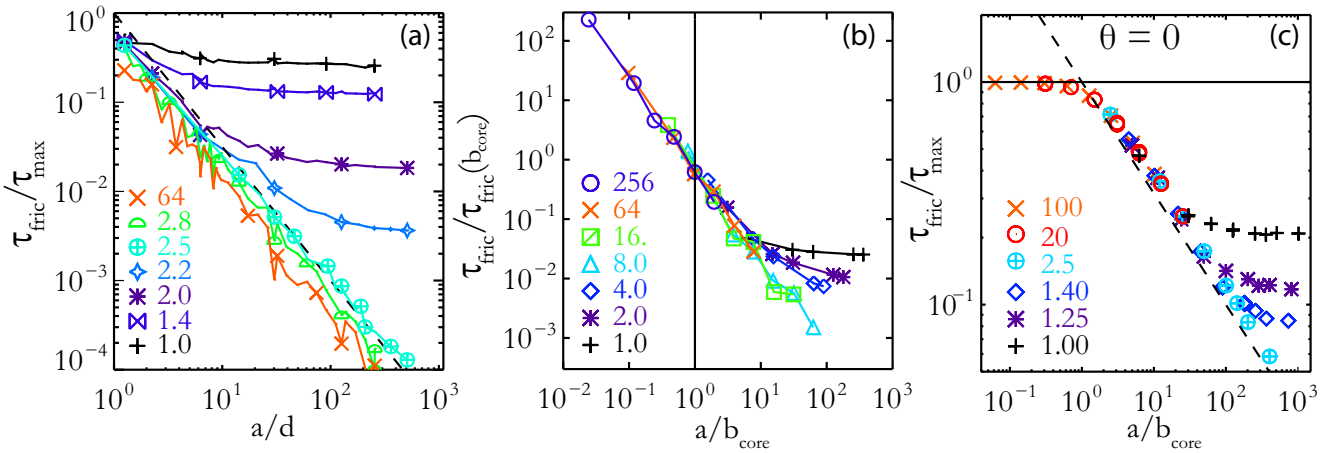

FIG. 2. Static friction stress vs contact radius for the values of b_{core}/d indicated by symbols in the legend. (a) For incommensurate contacts τ_{fric} decreases as $a^{-3/2}$ (dashed line) and then saturates at a plateau that decreases with increasing b_{core}. (b) Scaling by b_{core} and $\tau_{fric}(b_{core})$ shows that rigid scaling holds for $a < b_{core}$ and τ_{fric} saturates for $a \gg b_{core}$. The rotation angles are (a) 25° and (b) 3.4° to illustrate that similar behavior occurs for all incommensurate surfaces. (c) For commensurate ($\theta = 0°$) surfaces τ_{fric} is constant at $a < b_{core}$ and then drops as $a^{-1/2}$ to a plateau value that decreases with increasing b_{core}.

For the compliant case shown in Figs. 1(b) and 1(d), misregistry becomes localized into dislocation cores. Between dislocations the surfaces lock together to effectively resist sliding. As has been observed in the simpler case of 1D systems [14] and suggested for 2D systems [21,22], sliding occurs through dislocation motion along the interface rather than rigid translation of the entire surface. Contact produces an initial network of misfit dislocations. In the case shown, there were three horizontal dislocations separated by λ at locations where the force changes sign in the rigid case. The Supplemental Material [33] shows how these dislocations evolve during sliding. Sliding produces a nonuniform stress distribution with singularities near the edge of the contact [26], as discussed below. This causes the dislocations to curve as they move and nucleates new dislocations at the contact edge. Figure 1(b) shows a snapshot from steady state sliding. As sliding continues, the dislocations move inwards towards the central ellipse and annihilate while new dislocations nucleate at the edge. The number of dislocations at the peak force corresponding to static friction increases with a/b_{core}.

Figure 2(a) reveals how compliance affects the static friction. As G and b_{core} decrease, the friction deviates from the rigid scaling at smaller and smaller a. At large a the shear stress approaches a constant limiting value that increases as b_{core} decreases. Similar behavior is observed for all rotation angles that produce an incommensurate interface.

The importance of b_{core} is illustrated by the rescaled data for $\theta = 3.4^{\circ}$ in Fig. 2(b). The radius is normalized by b_{core} and the friction by the rigid prediction for $a = b_{\mathrm{core}}$. For $a < b_{\mathrm{core}}$ the stress exhibits the power law scaling predicted for rigid surfaces. For $a > b_{\mathrm{core}}$ dislocations can enter the contact and the interface deforms to lock into local registry. The friction is above the rigid prediction, dropping more slowly and then saturating at large a/b_{core}. Given our limited simulation size it is difficult to reach the asymptotic limit for $b_{\mathrm{core}} > 5d$, but the arguments below suggest that the saturating value drops exponentially with increasing b_{core}.

Previous work on interfacial dislocations in circular contacts between 3D solids [25,27,34] has focused on the commensurate case, $\theta = 0$. Results for this special case are shown in Fig. 2(c). Because all atoms are in phase in the rigid limit, the shear stress is independent of a. As a becomes larger than b_{core}, the friction drops below the rigid limit. The initial decrease scales as $a^{-1/2}$. As shown in a one-dimensional model by Hurtado and Kim [25], this can be understood from the fact that continuum theory predicts that a uniform displacement in the contact produces a singular shear stress at the edge of the contact. The stress within b_{core} of the edge scales as $(a/b_{\mathrm{core}})^{1/2}$ times the stress in the center. When this edge stress reaches $\tau_{\max}$, a dislocation can nucleate at the circumference and propagate across the interface, allowing the whole contact to advance by d. Gao has observed this regime [27] in two-dimensional simulations up to $a/b_{\mathrm{core}} \sim 50$ and Fig. 2(c) extends the scaling regime by more than an order of magnitude.

At very large a/b_{core}, many dislocations are stable in the contact. In this limit one expects [34] that the shear stress approaches the Peierls stress for dislocation motion τ_{Peierls}. Our simulations are large enough to access this regime, showing a clear saturation at a force that decreases with increasing b_{core}.

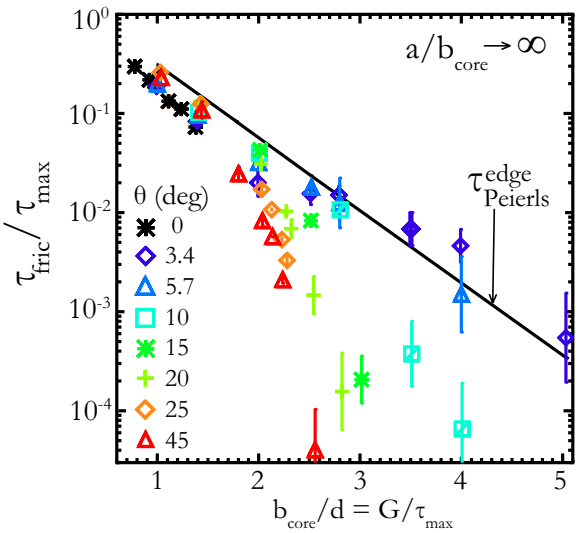

FIG. 3. Plateau stress for $a/b_{\mathrm{core}} \to \infty$ at the indicated rotation angles (symbols) and the Peierls stress for edge dislocations in a periodic system (solid line). There are significant error bars at large b_{core} where it is difficult to reach full saturation. The top of each error bar represents an upper bound corresponding to τ_{fric} at the largest a studied (512–1024d). The bottom was estimated by linearly extrapolating the tail of log-log plots as in Fig. 2 to ten times the largest a studied.

The results shown in Fig. 2 suggest that for both incommensurate and commensurate systems the shear stress in large contacts approaches the Peierls stress for dislocation motion. As shown in Fig. 1, dislocations make a loop and thus change from an edge character at the front and back, to screw dislocations at the sides. We performed a set of simulations with periodic boundary conditions to determine τ_{Peierls}. The same compliant substrate was used but the rigid periodic potential was stretched or skewed to impose a single dislocation per unit cell at the desired orientation. The stress on the top surface was then increased to determine the Peierls stress at which the dislocation moved. As predicted from continuum theory [35,36], $\tau_{\mathrm{Peierls}}/\tau_{\max} \propto \exp(-b_{\mathrm{core}}/d) = \exp(-G/\tau_{\max})$. The solid line in Fig. 3 shows a fit to data for an edge dislocation perpendicular to the sliding direction. Stresses for other orientations were both larger and smaller, but also show exponential scaling at large core widths.

Also shown in Fig. 3 are the saturation friction stresses for a wide range of θ and b_{core}. A striking conclusion is that similar physics determines the saturating stress in both commensurate and incommensurate contacts. In the limit of small θ or small b_{core}, commensurate and incommensurate surfaces have similar shear stresses that scale with the Peierls stress for a single edge dislocation. At larger θ and b_{core}, τ_{fric} is depressed and results for each θ seem to decay with a more rapid exponential. In this limit, local locking into the $\theta = 0$ commensurate state gives an intrinsic dislocation spacing $\lambda = d/\theta$ that is smaller than b_{core}. Interactions between nearby dislocations are known to reduce the effective Peierls stress. The system can also lock into a higher order commensurate state. Independent simulations of these states in systems with periodic boundary conditions show exponentially decaying frictional stresses that

are similar to the results in Fig. 3. There is no friction in the rigid limit ($b_{\rm core} \to \infty$), because our interfacial interaction is purely sinusoidal with no harmonics [12]. More realistic potentials lead to significant friction in the rigid limit.

Given the strong dependence of Peierls stress on $b_{\rm core}$ it is interesting to consider typical values for real materials. For contact between two identical solids, Eq. (1) should give a simple model for interactions between lattice planes in the bulk as well as at the interface. In this case, $G/\tau_{\rm max} \sim 2\pi h/d$, where h is the spacing between lattice planes. Our geometry is consistent with the (001) surface of an fcc crystal and thus $G/\tau_{\rm max} \sim 4.4$. Experimental studies of the friction force on islands may be able to reach scales where saturation to the Peierls stress can be observed [9]. The core width would be smaller and the Peierls stress much larger if the interaction between solids was stronger than the internal interactions. As noted by Müser [23], such interfaces are likely to be metastable against alloying. However, he found no mixing on simulation time scales for systems that would correspond to $b_{\rm core} \sim d$ where our calculated Peierls stress is large.

The directional covalent bonding in silicon and diamond can lead to large yield stresses and small dislocation core widths $b_{\rm core} \sim d$ [37,38]. As expected from Fig. 3, unpassivated incommensurate surfaces of these materials spontaneously deform to form an interface with a yield stress that is comparable to the bulk. Passivating the dangling covalent bonds at the surface with hydrogen reduces $\tau_{\rm max}$ to $\sim$ 10 MPa, which is characteristic of van der Waals interactions [39]. The resulting $b_{\rm core} \sim 10\ \mu$m and the corresponding Peierls stress would be below the limit of detection in practical experiments. Of course it is difficult to make crystalline surfaces of diamond and silicon that are atomically flat on this scale. For multiasperity rough contacts or disordered surfaces there can be a new mechanism of elastic pinning beyond an elastic correlation length determined by the competition between elasticity and the strength of disorder [40–43]. One source of disorder is the variation in phase and magnitude of friction forces from individual asperities such as those considered here.

Large atomically flat surfaces are readily obtained for layered materials such as MoS_2 and graphite. In these highly anisotropic materials, the width of interfacial dislocations is determined by the competition between stiff covalent bonds within layers and the weak van der Waals interactions between layers [44]. The value of $b_{\rm core}/d$ will be so large that the Peierls stress is negligible and this must contribute to the success of these materials as solid lubricants.

The results presented above provide insight into the competition between geometry, elasticity, and interfacial shear stress in determining the friction of two-dimensional contacts between crystalline three-dimensional solids. For small contact radii we find the friction scales according to previously derived rules for rigid solids. For commensurate surfaces there is a constant frictional stress, while $\tau_{\rm fric}$ decreases as a power of radius for incommensurate surfaces.

Elasticity becomes important when the radius exceeds the width of edge dislocation cores, $b_{\rm core} = dG/\tau_{\rm max}$. For commensurate surfaces, nucleation at the circular contact boundary leads to a universal decrease in stress as $\tau_{\rm fric} \sim (a/b_{\rm core})^{-1/2}$. The friction stress then saturates at the Peierls stress for dislocation loops to move across the interface. The stress also saturates at large $a/b_{\rm core}$ for incommensurate surfaces. Moreover, the Peierls stress is nearly the same for commensurate and incommensurate systems at small $b_{\rm core}$ and λ. This result is in stark contrast to the rigid limit [1–3,9]. In all cases studied the saturation stress drops exponentially with $G/\tau_{\rm max}$. Thus there is no true zero friction state, but the friction stress may be extremely small in stiff systems.

This material is based on work supported by the National Science Foundation under Grant No. DMR-1411144 and by the Deutsche Forschungsgemeinschaft (Grant No. PA 2023/2). Calculations were partially carried out at the Jülich Supercomputing Center (Project No. hfr13).

[1] M. Hirano and K. Shinjo, Phys. Rev. B **41**, 11837 (1990).
[2] M. Hirano, K. Shinjo, R. Kaneko, and Y. Murata, Phys. Rev. Lett. **67**, 2642 (1991).
[3] M. Hirano, in *Superlubricity*, edited by A. Erdemir and J.-M. Martin (Elsevier, Amsterdam 2007), Chap. 2, pp. 17–38.
[4] M. Dienwiebel, G. S. Verhoeven, N. Pradeep, J. W. M. Frenken, J. A. Heimberg, and H. W. Zandbergen, Phys. Rev. Lett. **92**, 126101 (2004).
[5] Z. Liu, J. Yang, F. Grey, J. Z. Liu, Y. Liu, Y. Wang, Y. Yang, Y. Cheng, and Q. Zheng, Phys. Rev. Lett. **108**, 205503 (2012).
[6] E. Koren, E. Lörtscher, C. Rawlings, A. W. Knoll, and U. Duerig, Science **348**, 679 (2015).
[7] X. Feng, S. Kwon, J. Y. Park, and M. Salmeron, ACS Nano **7**, 1718 (2013).
[8] M. Hirano, K. Shinjo, R. Kaneko, and Y. Murata, Phys. Rev. Lett. **78**, 1448 (1997).
[9] D. Dietzel, M. Feldmann, U. D. Schwarz, H. Fuchs, and A. Schirmeisen, Phys. Rev. Lett. **111**, 235502 (2013).
[10] D. Dietzel, C. Ritter, T. Mönninghoff, H. Fuchs, A. Schirmeisen, and U. D. Schwarz, Phys. Rev. Lett. **101**, 125505 (2008).
[11] J.-M. Martin, C. Donnet, T. Le Mogne, and T. Epicier, Phys. Rev. B **48**, 10583 (1993).
[12] M. H. Müser, L. Wenning, and M. O. Robbins, Phys. Rev. Lett. **86**, 1295 (2001).
[13] A. S. de Wijn, Phys. Rev. B **86**, 085429 (2012).
[14] O. M. Braun and Y. S. Kivshar, *The Frenkel-Kontorova Model: Concepts, Methods, and Applications* (Springer, Berlin, 2004).
[15] J. Ringlein and M. O. Robbins, Am. J. Phys. **72**, 884 (2004).
[16] M. H. Müser, M. Urbakh, and M. O. Robbins, Adv. Chem. Phys. **126**, 187 (2003).
[17] M. Cieplak, E. D. Smith, and M. O. Robbins, Science **265**, 1209 (1994).
[18] M. S. Tomassone, J. B. Sokoloff, A. Widom, and J. Krim, Phys. Rev. Lett. **79**, 4798 (1997).
[19] A. Liebsch, S. Goncalves, and M. Kiwi, Phys. Rev. B **60**, 5034 (1999).

[20] N. Varini, A. Vanossi, R. Guerra, D. Mandelli, R. Capozza, and E. Tosatti, Nanoscale **7**, 2093 (2015).
[21] J. Friedel and P.-G. de Gennes, Philos. Mag. **87**, 39 (2007).
[22] A. P. Merkle and L. D. Marks, Tribol. Lett. **26**, 73 (2007); Philos. Mag. **87**, 527 (2007).
[23] M. H. Müser, Tribol. Lett. **10**, 15 (2001).
[24] W. K. Kim and M. L. Falk, Phys. Rev. B **80**, 235428 (2009).
[25] J. A. Hurtado and K.-S. Kim, Proc. R. Soc. London, Ser. A **455**, 3363 (1999).
[26] K. L. Johnson, *Contact Mechanics* (Cambridge University Press, Cambridge, UK, 1985).
[27] Y. Gao, J. Mech. Phys. Solids **58**, 2023 (2010).
[28] L. Pastewka, T. A. Sharp, and M. O. Robbins, Phys. Rev. B **86**, 075459 (2012).
[29] R. W. Hockney, Methods Comput. Phys. **9**, 135 (1970).
[30] C. Campañá and M. H. Müser, Phys. Rev. B **74**, 075420 (2006).
[31] Note that for $\nu \neq 0.5$ frictional stresses change the lattice constant and thus the commensurability.
[32] S. J. Plimpton, J. Comput. Phys. **117**, 1 (1995).
[33] See Supplemental Material at http://link.aps.org/supplemental/10.1103/PhysRevB.93.121402 for movies showing the evolution of stress and dislocations in the contacts shown in Fig. 1.
[34] J. A. Hurtado and K.-S. Kim, Proc. R. Soc. London, Ser. A **455**, 3385 (1999).
[35] F. R. N. Nabarro, Mater. Sci. Eng., A **234-236**, 67 (1997).
[36] D. Hull and D. J. Bacon, *Introduction to Dislocations*, 5th ed. (Butterworth-Heinemann, Oxford, 2011).
[37] R. Choudhury, C. Gattinoni, G. Makov, and A. De Vita, J. Phys.: Condens. Matter **22**, 074210 (2010).
[38] W. Cai, V. V. Bulatov, J. Chang, J. Li, S. Yip, F. Nabarro, and J. Hirth, *Dislocation Core Effects on Mobility*, Vol. 12 (Elsevier, Amsterdam, 2004).
[39] G. Zilibotti and M. C. Righi, Langmuir **27**, 6862 (2011).
[40] A. Volmer and T. Natterman, Z. Phys. B **104**, 363 (1997).
[41] B. N. J. Persson and E. Tosatti, in *Physics of Sliding Friction*, edited by B. N. J. Persson and E. Tosatti (Kluwer, Dordrecht, 1996), pp. 179–189.
[42] C. Caroli and P. Nozieres, in *Physics of Sliding Friction*, edited by B. N. J. Persson and E. Tosatti (Kluwer, Dordrecht, 1996), pp. 27–49.
[43] M. H. Müser, Europhys. Lett. **66**, 97 (2004).
[44] T. Liang, W. G. Sawyer, S. S. Perry, S. B. Sinnott, and S. R. Phillpot, Phys. Rev. B **77**, 104105 (2008).